JOURNAL OF SOLID STATE CHEMISTRY **124,** 264–271 (1996)
ARTICLE NO. 0235

Ordering, Incommensuration, and Phase Transitions in Pyrrhotite

Part I: A TEM Study of Fe_7S_8

Fan Li and Hugo F. Franzen[1]

Ames Laboratory and Department of Chemistry, Iowa State University, Ames, Iowa 50011

and

Matthew J. Kramer

Ames Laboratory and Department of Geological and Atmospheric Sciences, Iowa State University, Ames, Iowa 50011

Received November 28, 1995; in revised form April 18, 1996; accepted April 23, 1996

Vacancy ordering in synthetic Fe_7S_8 at elevated temperature was studied using transmission electron microscopy. Two known idealized structures of Fe_7S_8 are monoclinic and trigonal based upon ABCD and ABC stacking of Kagome nets, respectively. The TEM results indicate a tendency for Fe_7S_8 to transform from monoclinic to trigonal between 200 and 300°C. A disordering of vacancies occurs above 300°C and yields a partially filled CdI_2-type structure. The Curie magnetic transition is associated with this vacancy-ordering transition. On slow cooling, it was found that the vacancies are ordered such as to tend to restore the Kagome nets and lead to ABCD and ABC layering.

1. INTRODUCTION

A primary feature of the vacancy ordering in defect NiAs-type iron sulfides is the formation of Kagome nets, partially vacant hexagonal planes of iron atoms within which vacancies are ordered such that they occupy the alternate sites in alternate rows (see Fig. 1a). Therefore, an understanding of the structures of the nonstoichiometric iron sulfides ($Fe_{1-x}S$) can be based upon consideration of the stacking sequences of Kagome nets along the *c* axis of NiAs-type substructure. Here the stacking sequence refers to two variations: (i) permutation of filled Fe and Kagome nets (at this point the origins of the Kagome net are considered as randomly located in the *a*–*b* plane); (ii) ordering of Kagome nets in the [001] direction (at this point the four possible origins in the Kagome nets are considered to be ordered along [001] direction when layering, i.e., the Kagome nets are labeled as A, B, C, and D).

[1] To whom correspondence should be addressed.

Among the defect iron sulfides that can be described as ordered vacancies in the NiAs-type structure, Fe_7S_8 is an extreme. This composition corresponds to Kagome nets alternating with filled planes, with 1/8 of the iron positions completely empty. As for the ordering of Kagome nets, although a variety of possible stacking sequences can be generated with little energy preference (1), only two sequences in Fe_7S_8, $D_AFD_BFD_CFD_DF \ldots$ and $D_AFD_BFD_CF \ldots$ (F: iron-filled layer, D_A, D_B, D_C, and D_D stand for the four Kagome nets unequivalent with respect to the origin), have been identified by X-ray diffraction studies. The former yields an ideal monoclinic symmetry with $c = 4C$ (see Fig. 1b), while the latter yields a trigonal structure with $c = 3C$ (*A* and *C* in this paper will refer to the *a* and *c* length of NiAs-type structure, respectively). It is noteworthy that the $4C$ monoclinic structure with ABCD stacking has been found only in natural pyrrhotite minerals that have undergone processes over geological time (2), and the $3C$ trigonal structures were only found in quenched samples (3, 4). The relationship of these two structures has not been studied, so it has remained unclear whether the $3C$ stacking is an intermediate superstructure phase stable at certain temperatures or forms as a metastable phase. As for the laboratory-grown samples, mixed stacking of both ABC and ABCD is most often encountered. Samples prepared in our laboratory and elsewhere have been found to be badly twinned to X rays. In order to refine the X-ray diffraction of a single crystal of Fe_7S_8, Keller-Besrest *et al.* (5) introduced a fault rate for the $4C$ stacking sequence to rationalize the partial occupancy variable and in this way obtained a very good solution. Furthermore, the mixing of stacking sequences of Kagome nets can vary from random through incommensurate to complete order in domains of the dimensions appropriate to X-ray or TEM investigation, and

0022-4596/96 $18.00

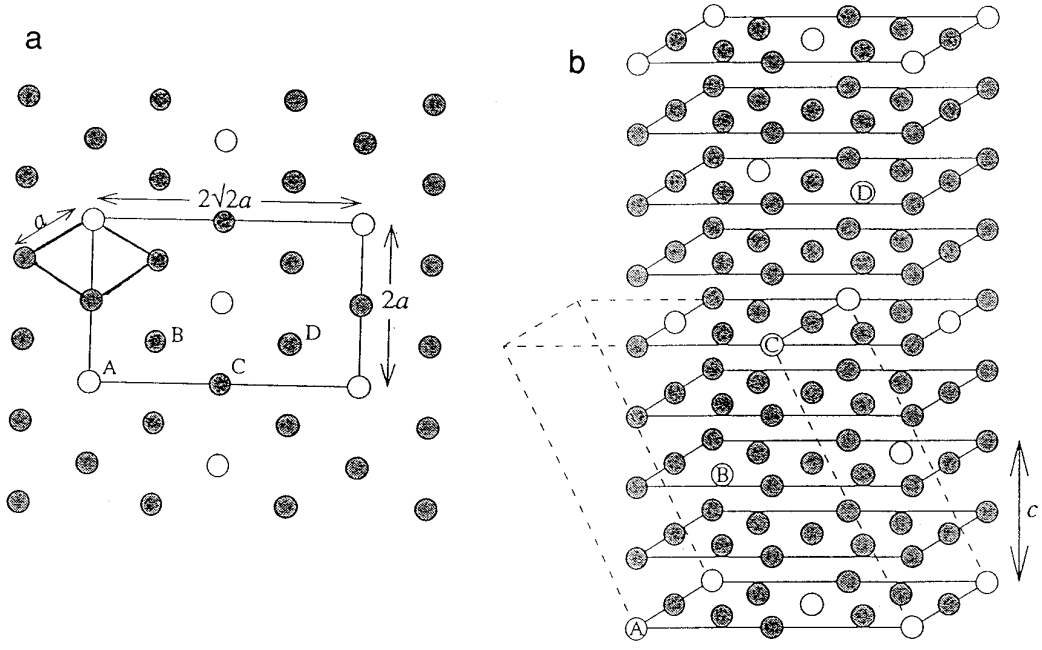

FIG. 1. (a) A schematic Kagome net in NiAs-type $Fe_{1-x}S$. The open circles represent the vacancy sites and the solid circles represent the iron-filled sites. Notice that for a subcell shown by the bold lines there are four unequivalent sites as labeled as A, B, C, and D for which the vacancies could be placed. The superstructure derived from such a Kagome net will have the lattice parameters $A = 2\sqrt{2}a$ and $B = 2a$ (a and c refer to the lattice parameters of a NiAs subcell) as illustrated by the lighter lines. (b) In Fe_7S_8, the Kagome nets are stacked alternately with the iron filled layers along the c axis and the A, B, C, and D nets are staggered such that a $4C$ monoclinic structure results. The dash lines show such a monoclinic unit cell where the sulfur atoms are omitted for simplicity.

this disorder can be of thermodynamic or kinetic origin. These complications have hindered the understanding of phase relations in this system.

In the study of structural imperfection, electron diffraction is of special interest due to its high sensitivity in comparison with X rays, allowing the examination of a thin section of specimen and providing evidence of ordering on a smaller scale (by a factor of 10^3 or more). In the past decades, several attempts have been made to shed further light on the pyrrhotite structures using TEM (6–8), but almost all the crystals studied were naturally occurring $Fe_{1-x}S$. The samples invariably gave evidence for twinning, heterogeneity, or composition gradients. It is known that Fe_7S_8 is ferrimagnetic because of vacancy ordering within the alternate layers along the c axis and an antiferromagnetic coupling between the adjacent planes at room temperature, and it is further known that this material transforms to paramagnetic at about 315°C. It has, however, not been demonstrated whether this transformation results from disordering of vacancies or from a magnetic moment disordering process.

The present paper reports the results of a TEM study that was carried out on a synthetic Fe_7S_8 sample in order to improve our understanding of the relationship between the monoclinic and trigonal forms of pyrrhotite, and of the relationship between the magnetic transition and the ordered structure. In this work we have attempted to attach significance only to what can be readily distinguished. Among the stacking sequences described above, only the trigonal (ABCABC . . .) doubles the basal plane periods in the projection down the c axis. A crystal that was generally expected, and on the basis of diffraction patterns and lattice images confirmed, to be the monoclinic structure was observed via diffraction patterns to transform at 205°C to yield diffraction maxima that double a and b in projection down the c axis. At this temperature an endothermic effect was observed (by DTA) upon heating a bulk sample and the sample is known to be ferrimagnetic. Taken together these diffraction, thermal, and magnetic effects point to, at least partial, ABCABC . . . ordering with increasing temperature, and thus to reversible development of this ordering in pyrrhotite.

2. EXPERIMENTAL

Fe_7S_8 was synthesized from high purity iron (Johnson–Matthey, 5N, −20 mesh) and sulfur (Aldrich, sublimed, −100 mesh) powders; the latter was pressed into pellets before mixing with iron powder. Carefully weighed quantities of iron and sulfur were sealed in evacuated silica-glass tubes and were then placed into a tube furnace. The heating and annealing procedure was as follows: The samples were

at first heated to 410°C and then gradually to 500°C. As sulfur vaporized over this temperature range, it diffused to the cooler end of the silica tube where the iron powder was placed so that the reaction between these two elements could take place. The temperature was controlled below 500°C until no yellow sulfur vapor was visible (approximately 1 week), and then annealed at 700–800°C for 20 days. Finally, the samples were cooled at a rate of 5°C/h to room temperature with pauses for 2 days at 310°C and at 130°C.

The compositions of the final products were verified using the electron microprobe (ARL, SEMQ). The operating conditions were 20 kV accelerating voltage and 25 nA beam current. Under these conditions both Fe and S were determined on WDS spectrometers (LiF crystal for Fe, PET crystal for S), and count rates were about 10,000 s^{-1}. Three samples, $Fe_{0.885}S$, $Fe_{0.967}S$, and $Fe_{0.980}S$, prepared by Dr. Paul G. Spry (9) were used for standards. The theoretical error from counting statistics for a counting time of 10 s was about 0.3%; the actual reproducibility as determined by a series of counts on the standards usually gave standard deviations of 0.6 to 0.8%. The compositional variations in different areas of the sample were found to be within these limits. Thus the standard deviation of the measured stoichiometry was lower than 1%, and the good sample homogeneity was further indicated by the absence of any significant anticorrelation between measured concentrations of Fe and S. Finally, only samples with the Fe/S ratio = 7/8 and satisfactory homogeneity were used for this study.

For the TEM observations the sample was crushed in a mortar and pestle into <400 mesh and mixed with ethanol. A single drop of the suspension was placed onto a holey carbon grid and allowed to air dry. Once dried, the sample was examined using a Philips CM30 TEM with a heating stage. All the selected area diffraction patterns in Fig. 3 were obtained from the same region of the crystal using a 50 μm aperture (i.e., the region near the tip of the crystal indicated by an arrow in Fig. 7a). *In situ* heating was performed using a double tilt hot stage (Gatan, Model 628-0500) with a temperature monitor and a Pt/Rh thermocouple mounted at the edge of the sample. The heating current was manually adjusted, and the measured temperature, according to prior calibration, is within ±10°C of the sample temperature. Since the sample had been confirmed to have a Curie transition at 315°C, the highest heating temperature was 340°C.

A differential thermal analysis (DTA) was carried out using a Perkin–Elmer DTA 1700 with a System 7/4 thermal controller. The sample powder was loaded into an alumina

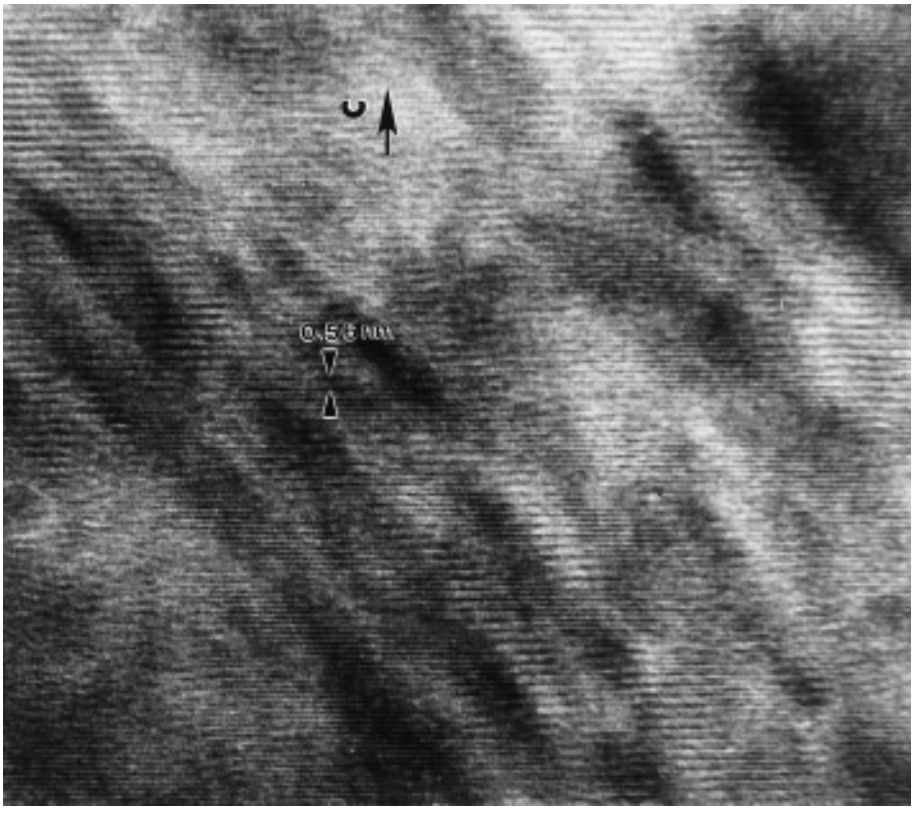

FIG. 2. A HRTEM image for the Fe_7S_8 sample at room temperature with the electron beam perpendicular to the *c* axis.

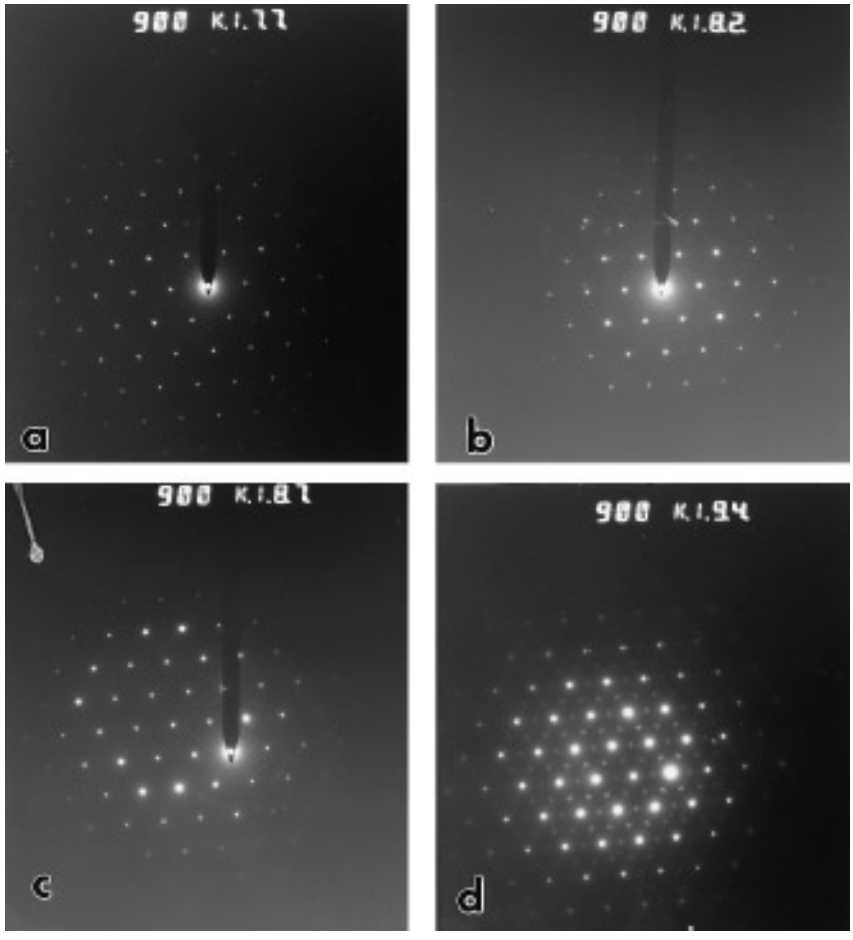

FIG. 3. SAD patterns for the $[001]_{NiAs}$ zone. Notice that all the patterns were obtained from the same region of the crystal (i.e., the region near the tip of the crystal as shown by an arrow in Fig. 8A). (a) at room temperature; (b) at 210°C; (c) at 340°C; (d) when cooled to room temperature.

crucible. The heating and cooling rates were 5 K/min under the Ar-gas flow with O_2 impurity <40 ppm.

3. RESULTS AND DISCUSSIONS

3.1. The Structure at Room Temperature

The alternation of partially filled Kagome net layers with the fully filled iron layers can be clearly seen in the high resolution transmission electron micrography (HRTEM). Figure 2 depicts a layer image from the Fe_7S_8 sample at room temperature with the electron beam perpendicular to the *c* axis. The fringes show a contrasting alternation of a dark strip with a light strip, indicating a two-layer periodicity. The distance between two dark strips was estimated to be d = 5.6–5.7 Å which corresponds to one *c* length of the NiAs-type substructure. From this view, however, the monoclinic and trigonal orderings are indistinguishable, as, in fact, are the projected Kagome nets. Figure 3 displays a series of the $[001]_{NiAs}$ selected area diffraction patterns (SAD) at various temperatures. The pattern, when the sample was at room temperature, showed no weak superstructure reflections (Fig. 3a), and all the diffraction maxima in this projection corresponded to the NiAs substructure, suggesting that *a* and *b* axes are not doubled as they would be in the projected $2A \times 2A \times 3C$ trigonal structure. On the other hand, the convergent beam electron diffraction (CBED), as shown in Fig. 4, reveals a deviation from the hexagonal and trigonal symmetries in this direction. The observation that both the zero order Laue zone (ZOLZ) (central bright area) and the first order Laue zone (FOLZ) (outer thin ring) are coaxial indicates that the beam direction lies along the $(001)_{NiAs}$ axis. By looking at the changes in the intensity of ZOLZ and FOLZ, it can be found that the brightness of FOLZ is not uniform and the $(0\bar{4}40)_{NiAs}$ reflection in ZOLZ is very weak in comparison with $(40\bar{4}0)_{NiAs}$ and $(\bar{4}400)_{NiAs}$ reflections. This distribution in the reflection intensity implies the absence of hexagonal/trigonal symmetry, but the occurrence of a twofold axis whose direction

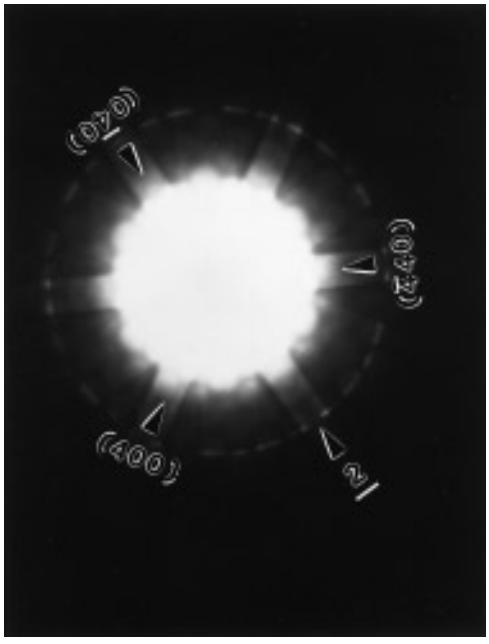

FIG. 4. CBED pattern of Fe_7S_8 from the $[001]_{NiAs}$ zone direction.

is arrowed in Fig. 4. We were unable to orient the sample for a good quality SAD in any $[hk0]_{NiAs}$ zone direction due to the restrictions on the degree of tilting the crystal, but the SAD for the $[012]_{NiAs}$ zone axis clearly exhibited a 4*C* superstructure (notice that 3 weak reflection spots lie between NiAs-type sublattice maxima $(0000)_{NiAs}$ and $(20\bar{2}\bar{1})_{NiAs}$) and all the reflections could be indexed according to the monoclinic structure (Fig. 5). The sublattice parameters measured from these SAD patterns are a = 3.44 Å and c = 5.68 Å which are in very good agreement not only with the spacing between the dark strips in Fig. 2, but also with what has been observed using XRD techniques.

A basic distinction between the monoclinic and trigonal structures of Fe_7S_8 is the difference in the vacancy density projected down the NiAs-type *c* axis. In the case of the ideal ABCD monoclinic structure the doubling of **a** and **b** inherent in the Kagome net is lost in the projection. Therefore, the projections of ideal monoclinic pyrrhotite in this zone show no superstructure, whereas in the ideal ABC trigonal case a doubling of the cell edges would be observed. This feature of the distinct SAD patterns was simulated very well by the computer program (Microscopist). Figure 6 displays the computer-generated SAD patterns for both the ideal ABCD and ABC stacking cases on the basis of the structural information provided in literature (2, 4).

Thus the above observations, i.e., (i) alternating density along the *c* axis, (ii) no superstructure in projection down *c* axis, and (iii) 4*C* superstructure reflections in the $[012]_{NiAs}$ zone direction, are all consistent with the interpretation that the known monoclinic structure of Fe_7S_8 is the stable modification at room temperature. It can, however, be concluded that the extent of monoclinic distortion in the synthetic sample is significantly lower than that found in natural samples, i.e., the lattice distortion is minimal and the observed monoclinic structure is present on a nearly undistorted hexagonal lattice.

3.2. Order–Disorder Transition at Elevated Temperature

When the sample temperature was raised to 210°C, and the $[001]_{NiAs}$ SAD pattern observed, in spite of presence

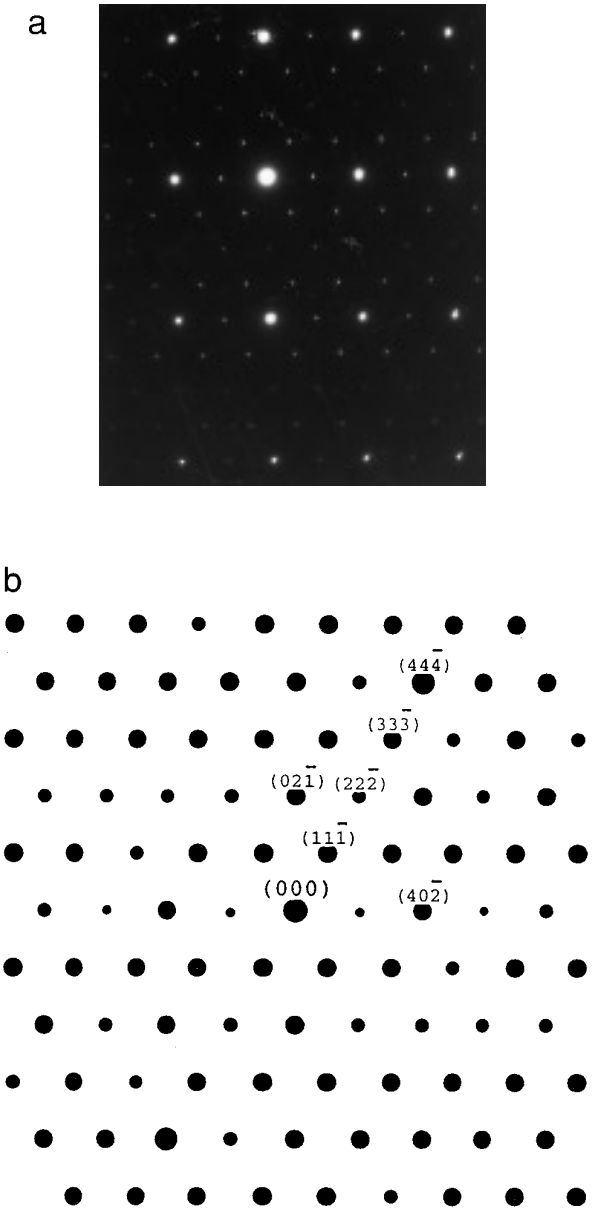

FIG. 5. (a) SAD pattern for the $[012]_{NiAs}$ zone and (b) the computer-generated pattern (× 1.5) for same zone axis based on the monoclinic structure where the indices refer to the monoclinic structure.

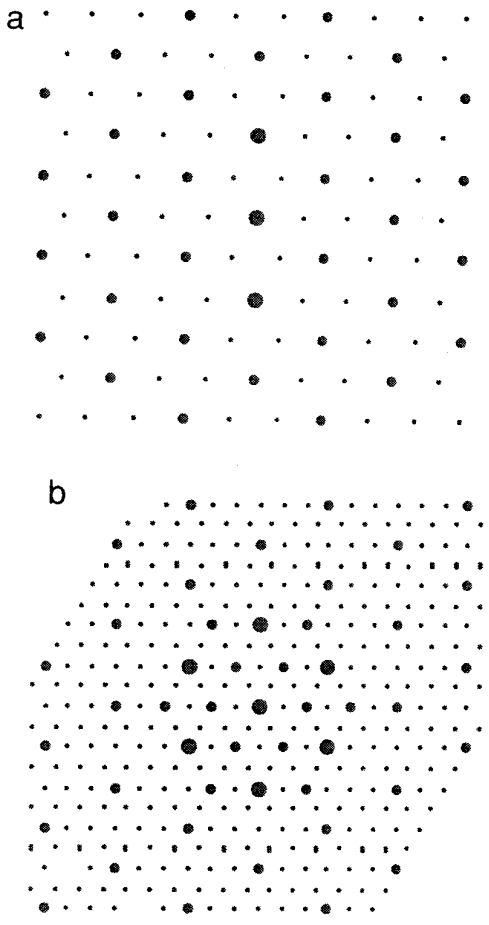

FIG. 6. (a). A SAD pattern from the $[001]_{NiAs}$ direction simulated for the monoclinic structure with the ABCD stacking. The space group is $C2/c$, and the structural information reported in Ref. (2) is used. Notice that this pattern shows no superlattice reflection. (b) A SAD pattern from the $[001]_{NiAs}$ direction simulated for the trigonal structure with the ABC stacking. The space group is $P3_121$, and the structural information reported in (3) is used. Notice that this pattern shows superlattice spots resulting in a doubling of a and b axis length.

of some randomly distributed reflection spots, a set of very weak spots was found to appear systematically between pairs of reflection maxima of the NiAs-type substructure. This observation can be interpreted as the formation of superstructure with doubled a and b length over a depth suitable for diffraction. However these weak superlattice spots were no longer observed when the temperature reached 340°C (Fig. 3b and 3c). These changes show that some superlattice with doubled a and b axes was developed and subsequently destroyed in the course of heating the sample. This development and destruction of $2A \times 2A$ superlattice in projection upon heating indicates that some trigonal ABC ordering in Fe_7S_8 occurs between room temperature, where the monoclinic is stable, and 340°C, where the vacancies disorder. These observations also show that at these relatively low temperatures a two-phase equilibrium mixture is not achieved, but rather a mixing of stacking sequences occurs. Because the XRD patterns at 350°C showed superstructure diffraction peaks at low angle of 2θ, and because a rapid increase of magnetization was found upon cooling samples heated to 340°C (10), it is concluded that the vacancies do not disorder to yield a NiAs-type structure at this temperature but rather remain in a ··· DFDFDFDF ··· stacking sequence (D: iron deficient plane with randomly distributed vacancies; F: iron filled plane) along the c axis that results in a partially filled CdI_2-type symmetry. Therefore, the proposed transition sequence along the temperature scale is: monoclinic (ABCD) → trigonal (ABC) → defect CdI_2-type with a DFDF stacking.

The heat effects accompanying these transitions were observed during a DTA experiment on this synthetic Fe_7S_8 sample. Figure 7 shows the DTA curves corresponding to heating from 50 to 400°C and subsequent cooling from 400 to 50°C. A small peak can be found at about 240°C, and a large peak follows at about 310°C. These results indicate that at the DTA heating and cooling rates the sample undergoes two changes in structural modification, one corresponding to, as proposed, the monoclinic → trigonal transition (or better disordered monoclinic → disordered trigonal) probably in a wide temperature range between 200 and 250°C, and the other corresponding to the vacancy-

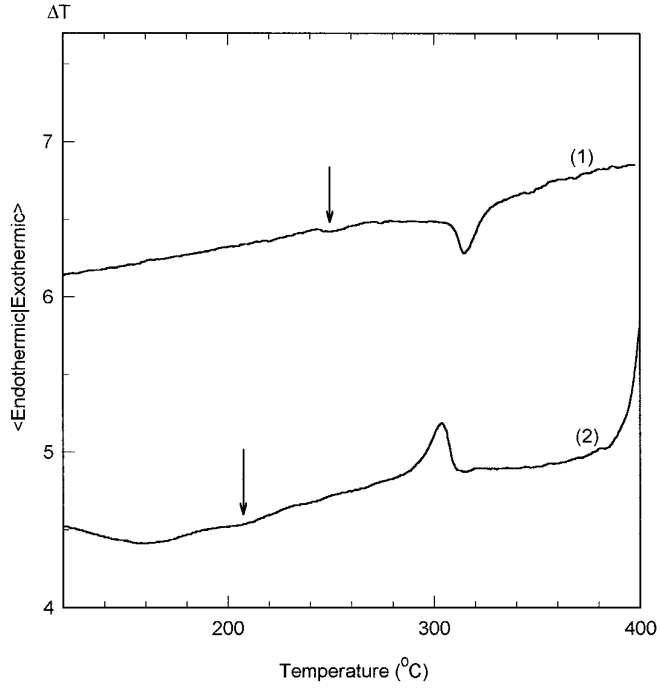

FIG. 7. DTA curves of the synthetic Fe_7S_8 sample. Curve 1: heating from 50 to 400°C at + 5 K/min. Curve 2: cooling from 400 to 50°C at −5 K/min. The small anomalies are indicated by arrows.

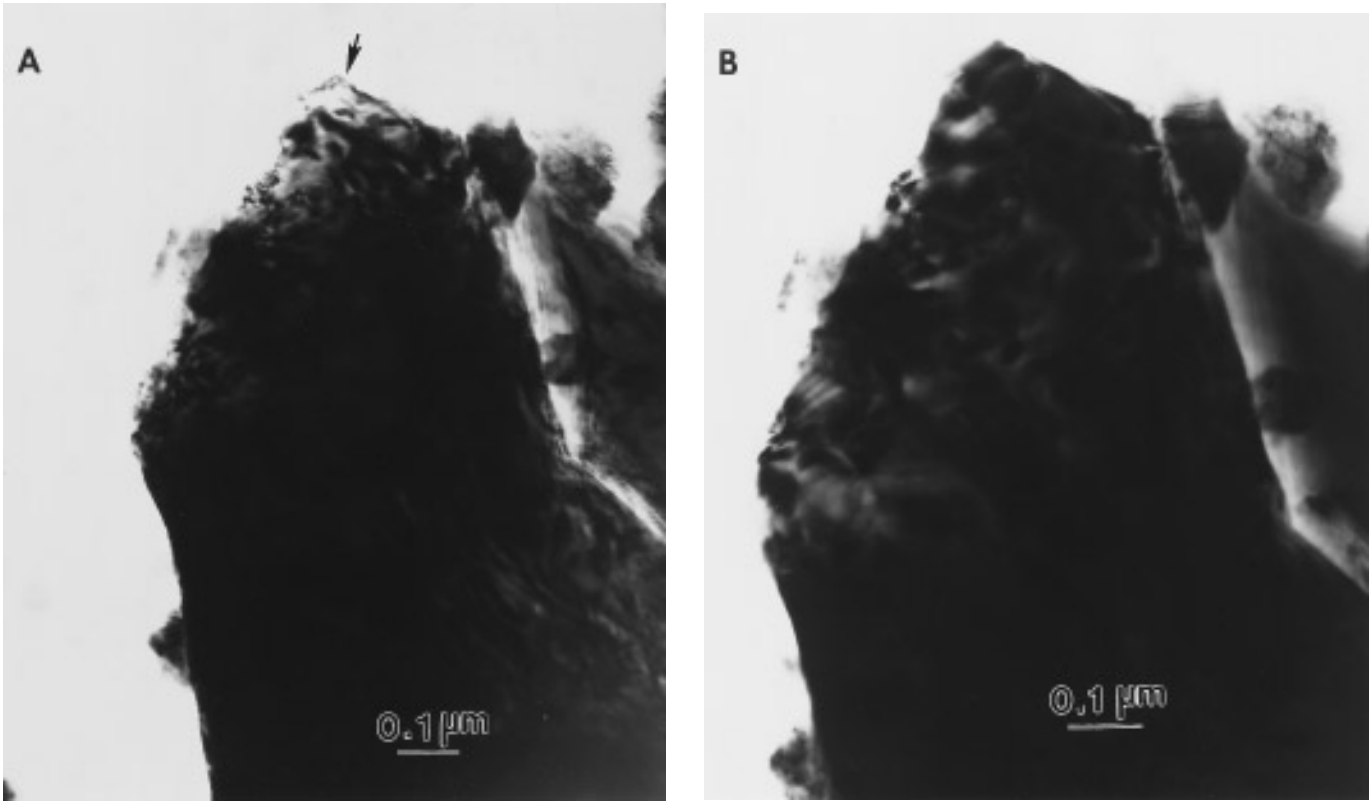

FIG. 8. TEM images (A) at room temperature; (B) at 210°C; (C) at 340°C; (D) when the sample was cooled to room temperature.

disordering transition in a narrow temperature range from 305 to 320°C. Also, the transitions in these two temperature ranges were observed from the thermal-magnetization and high-temperature X-ray diffraction investigations as will be reported in a separate paper.

3.3. SAD Pattern after Quenching Samples

When the sample was quenched from 340°C to room temperature in a few minutes, the SAD in the projection down the $[001]_{NiAs}$ direction demonstrated a relatively complicated Kagome pattern (Fig. 3d). A set of split spot pairs is displayed symmetrically at 1/2 ($\mathbf{a}^* + \mathbf{b}^*$) $\pm \delta$ relative to $n/2$ $\mathbf{a}^*$ and $n/2$ $\mathbf{b}^*$ (n = odd). These split diffraction spots indicate that a discommensuration occurs in the [001] plane when the sample is quenched on this time scale. The absence of this discommensuration in the as prepared samples shows that the annealing procedures used in the initial preparation yields predominantly the monoclinic ordered structure (although not ordered to the extent of natural samples). The doubling of the a and b axes in the $[001]_{NiAs}$ projection in the quenched sample indicates the formation of Kagome nets within the vacancy containing layers without the formation of the monoclinic ordering along the $[001]_{NiAs}$ direction, while the discommensuration suggests the existence of domains at relative long intervals along the $[110]_{NiAs}$ and $[1\bar{2}0]_{NiAs}$ directions. Such domains would result from periodic mixing of ABC trigonal stacking adjacent to ABCD monoclinic stacking with boundaries perpendicular to the $[110]_{NiAs}$ and $[1\bar{2}0]_{NiAs}$ directions and period appropriate to the length of 1/2 ($\mathbf{a}^* + \mathbf{b}^*$) $\pm \delta$ (δ was measured to be 5.91×10^{-3} Å^{-1}, which corresponds to a length of 169 Å (~50a)).

Quenching the disordered structure from high temperatures shows the strong tendency toward the formation of Kagome nets. The subsequent stacking of the Kagome nets depends on the temperature and cooling rate. However, it seems that the ABC sequence is more favored by rapid cooling. By using X-ray diffraction Fleet (3) investigated the structure of Fe_7S_8 samples prepared by quenching from 500°C, and found that crystals were twinned in such a way that domains were rotated by multiples of 60° about the c axis, as is the case with mixing of ABC and ABCD stacking. Thus, the results from both the X-ray and electron diffraction support the transition sequence proposed above, and are consistent with a kinetic barrier in the course of the transition from ABC stacking to ABCD stacking that was partially overcome in the samples annealed in the preparation of materials for this study, and such as are frequently found in natural occurring samples.

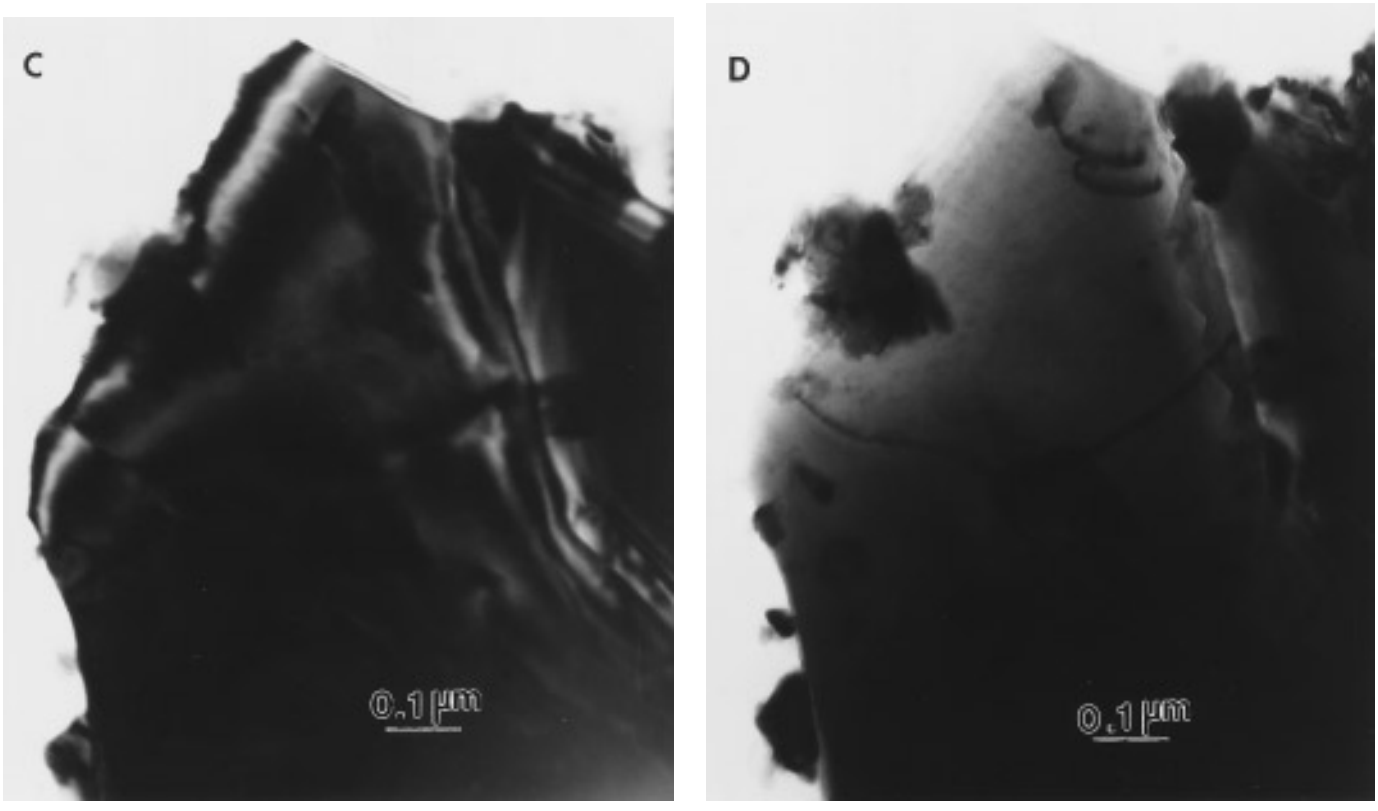

FIG. 8—*Continued*

3.4. Transmission Electron Micrographs

On the other hand, TEM images revealed a change of microstructure with temperature. At room temperature the grains in the sample are highly faulted, most likely due to annealing and cooling during sample preparation (Fig. 8A). As discussed above, the stacking sequence probably varies from one domain to another. As the temperature was raised, the observed strain contrasts became diffuse and vanished with the disappearance of the defects (Figs. 8B and 8C), implying that the disordering of vacancies has developed, so that the microstructure tends to reach a unified stacking sequence. After the sample is quenched, large size domains with the uniform microstructure are maintained, but some dislocations were observed (Fig. 8D).

4. CONCLUSION

The structures in Fe_7S_8 result from closely related stacking sequences of Kagome nets in alternate metal-containing layers along the *c* axis. Monoclinic ABCD layering is found at room temperature in well-annealed samples. Trigonal ABC layering tends to form at about 210°C, and remains up to about 300°C, above which the sample has a partially filled CdI_2-type structure, i.e., Fe-site vacancies distributed randomly within alternate layers of the NiAs-type. The Curie transition at 315°C is apparently associated with disordering of the vacancies.

ACKNOWLEDGMENTS

The authors express their thanks to Dr. Alfred Kracher for the EMP analysis work, to Dr. L. Scott Chumbley for his help and valuable suggestion in the electron diffraction experiment, and to Mr. Kevin Dennis and Mr. Hengning Wu for their help in the DTA experiments. This research was supported by the Office of the Basic Energy Sciences, through Materials Sciences Division, Ames Laboratory-operated for the U.S. Department of Energy by Iowa State University under Contract W-7405-Eng-82.

REFERENCES

1. M. Posfai and I. Dodony, *Eur. J. Mineral.* **2,** 525 (1990).
2. M. Tokomi, K. Nishiguchi, and N. Morimoto, *Am. Mineral.* **57,** 1066 (1972).
3. M. E. Fleet, *Acta Crystallogr. B* **27,** 1864 (1971).
4. A. Nakano, M. Tokonami, and N. Morimoto, *Acta Crystallogr. B* **35,** 722 (1979).
5. F. Keller-Besrest, G. Collin, and R. Comes, *Acta Crystallogr. B* **38,** 296 (1982).
6. H. Nakazawa, N. Morimoto, and E. Watanabe, *Acta Crystallogr. B* **35,** 722 (1979).
7. H. Nakazawa, N. Morimoto, and E. Watanabe, *Acta Crystallogr. A Suppl.* **31,** 722 (1975).
8. I Dodony and M. Posfai, *Eur. J. Mineral.* **2,** 529 (1990).
9. L. T. Bryndzia, S. D. Scott and P. G. Spry, *Econ. Geol.* **83,** 1193 (1988).
10. A paper submitted along with this paper.